

ORIGINAL RESEARCH

OPEN ACCESS



Markers of tumor-associated macrophages and microglia exhibit high intratumoral heterogeneity in human glioblastoma tissue

Mikael Ispirjan^{a,b,c,*}, Sascha Marx^{a,d,*}, Eric Freund^{b,e}, Steffen K. Fleck^a, Joerg Baldauf^a, Karl Roessler^e, Henry W. S. Schroeder^a, and Sander Bekeschus^{b,f}

^aDepartment of Neurosurgery, Greifswald University Medical Center, Greifswald, Germany; ^bZIK plasmatis, Leibniz Institute for Plasma Science and Technology (INP), Greifswald, Germany; ^cDepartment of Cardiology, Heidelberg University Hospital, Heidelberg, Germany; ^dDepartment of Cancer Immunology and Virology, Dana-Farber Cancer Institute, Harvard Medical School, Boston, MA, USA; ^eDepartment of Neurosurgery, Medical University of Vienna, Vienna, Austria; ^fDepartment of Dermatology and Venerology, Rostock University Medical Center, Rostock, Germany

ABSTRACT

Background: Human glioblastoma multiforme (GBM) is a highly aggressive tumor with insufficient therapies available. Especially, novel concepts of immune therapies fail due to a complex immunosuppressive microenvironment, high mutational rates, and inter-patient variations. The intratumoral heterogeneity is currently not sufficiently investigated.

Methods: Biopsies from six different locations were taken in a cohort of 16 GBM patients who underwent surgery. The tissue slides were analyzed utilizing high-content imaging microscopy and algorithm-based image quantification. Several immune markers for macrophage and microglia subpopulations were investigated. Flow cytometry was used to validate key results. Besides the surface marker, cytokines were measured and categorized based on their heterogeneity and overall expression.

Results: M2-like antigens, including CD204, CD163, Arg1, and CSF1R, showed comparatively higher expression, with GFAP displaying the least intratumoral heterogeneity. In contrast, anti-tumor-macrophage-like antigens, such as PSGL-1, CD16, CD68, and MHC-II, exhibited low overall expression and concurrent high intratumoral heterogeneity. CD16 and PSGL-1 were the most heterogeneous antigens. High expression levels were observed for cytokines IL-6, VEGF, and CCL-2. VILIP-a was revealed to differentiate most in principle component analysis. Cytokines with the lowest overall expression, such as TGF- β 1, β -NGF, TNF- α , and TREM1, showed low intratumoral heterogeneity, in contrast to β NGF, TNF- α , and IL-18, which displayed high heterogeneity despite low expression.

Conclusion: The study showed high intratumoral heterogeneity in GBM, emphasizing the need for a more detailed understanding of the tumor microenvironment. The described findings could be essential for future personalized treatment strategies and the implementation of reliable diagnostics in GBM.

ARTICLE HISTORY

Received 2 March 2024
Revised 18 September 2024
Accepted 30 October 2024

KEYWORDS

Brain cancer; HCI; high-content imaging; patients; TAM

Introduction


Tumors of all types, especially gliomas, have distinct intra- and inter-tumor heterogeneity.^{1,2} Uncovering the interrelationships of the tumor microenvironment is essential for understanding the tumor and its progression. Most studies with human tumor samples show their limitations exactly at this point. Often, a tumor is analyzed and histologically processed using only one sample from a single sampling site. The conclusions drawn from this are then applied to the entire tumor. However, it remains unconsidered whether the tumor is composed differently in different localizations. This plays a central role, especially concerning new immunotherapeutic approaches.

As the most malignant and aggressive brain tumor, glioblastoma multiforme (GBM) is also the most common primary malignant brain tumor. Despite a low incidence of 4–5/100,000 inhabitants, glioblastoma is a major health burden due to its

poor prognosis.³ The onset of glioblastoma is possible at any age, with the prevalence increasing with age. The median of occurrence is 64 years.⁴ Despite all image morphological approaches, the diagnosis of a glioblastoma is made histomorphologically. Tumor samples acquired intraoperatively underwent conventional histomorphological diagnostics, accompanied by fluorescence in situ hybridization (FISH), microsatellite PCR, and next-generation sequencing.⁵ This comprehensive approach aims to categorize the samples into the five distinct WHO subtypes, also with respect to their IDH status.⁶ Furthermore, morphological tumor phenotypes can be described, especially the perivascular GBM phenotype, the hypoxic GBM phenotype, and the invasive GBM phenotype.⁷ As cytokines are secreted by the tumor cells and can flow even before the BBB becomes dysfunctional, circulating immune cells can be mobilized.⁸

CONTACT Sascha Marx ✉ Sascha.Marx@med.uni-greifswald.de Department of Neurosurgery, Greifswald University Medical Center, Sauerbruchstr., Greifswald 17475, Germany; Sander Bekeschus ✉ Sander.Bekeschus@inp-greifswald.de ZIK plasmatis, Leibniz Institute for Plasma Science and Technology (INP), Felix-Hausdorff-Str. 2, Greifswald 17489, Germany

*authors contributed equally as second authors.

 Supplemental data for this article can be accessed online at <https://doi.org/10.1080/2162402X.2024.2425124>

© 2024 The Author(s). Published with license by Taylor & Francis Group, LLC.

This is an Open Access article distributed under the terms of the Creative Commons Attribution-NonCommercial License (<http://creativecommons.org/licenses/by-nc/4.0/>), which permits unrestricted non-commercial use, distribution, and reproduction in any medium, provided the original work is properly cited. The terms on which this article has been published allow the posting of the Accepted Manuscript in a repository by the author(s) or with their consent.

The recruited tumor-associated macrophages, microglial cells, and other non-neoplastic cells take on immunosuppressive properties and secrete soluble factors that often secrete a non-immunogenic tumor microenvironment.^{7,9} In hypoxic tumors, the necrotic tissue is frequently surrounded by tumor cells in the form of a pseudo palisade.¹⁰ As a result of the lack of oxygen, the proliferation rate decreases. Still, the expression of vascular factors is the hypoxia-inducible factor (HIF1 α)¹¹ and other genes that can increase radio- and chemo-resistance.^{12,13} The invasive phenotype is characterized by the excessive invasion of tumor cells or fiber tracts in the surrounding matter and basement membranes.¹⁴ Therefore, gross total resections are made impossible,¹⁵ and tumors can even penetrate the BBB.¹⁶

Approximately 30–50% of the cells in GBM consist of tumor-associated macrophages (TAM).^{17,18} Most studies indicate that a high number of TAM promote tumor growth and is associated with a poor prognosis.¹⁹ A distinction is made between mobile macrophages, which migrate from the blood, and resident tissue macrophages.²⁰ While mobile macrophages are derived from medullary monocytes, tissue macrophages develop from the yolk sac during embryogenesis.^{21–23} The resident tissue macrophages of the brain are called microglial cells.²⁴ The total TAM population is composed of approximately 85% infiltrating mobile macrophages and 15% microglial cells.²⁵ Most infiltrating macrophages are localized perivascular, whereas microglial cells are highly expressed primarily peritumorally.¹⁸ Traditionally classified into pro-inflammatory M1 and anti-inflammatory M2 phenotypes, recent studies reveal this binary classification to be overly simplistic.²⁶ Both microglia and macrophages in glioblastoma exhibit markers of M1, M2, and non-polarized M0 states.²⁷ Single-cell analyses show TAMs in glioblastoma display a dynamic identity, with a pro-inflammatory profile in the tumor core and an anti-inflammatory state in the periphery.²⁸ Glioblastoma exhibits significant spatial heterogeneity in its transcriptional programs. Different regions within the tumor show distinct gene expression profiles, which are influenced by factors such as hypoxia and the immune microenvironment.²⁹ The most recent studies emphasize the role of metabolic alterations and immune cell interactions in the progression of GBM.³⁰ Hypoxia-driven metabolic changes and epigenetic modifications contribute to the adaptive capabilities of glioblastoma cells, facilitating their survival and resistance to treatments.³⁰

This study analyzed glioblastoma inpatient and interpatient heterogeneity based on expression marker profiling of different cell types and secretion profiles of cytokines and chemokines, and quantitatively assessed similarities and differences for each data set and between both data sets. Key findings were CD16 and β NGF being the most and GFAP and BDNF, the least heterogeneity marker expressed or cytokines released among all markers and cytokines studied.

Methods

Human samples and tissue preparation

Eleven out of sixteen patients presenting with suspected glioblastoma underwent embedding and immunofluorescence

staining procedures. The exclusion of five patients resulted from divergent treatment approaches during method development. The local ethics committee approved the study (BB089/08b), and written informed consent was obtained from every participating GBM patient and control participant. The methods used in this work were carried out in accordance with the approved guidelines, with written informed consent obtained from all subjects. Clinical characteristics are summarized in (Table S1). Patient selection followed a pre-defined inclusion and exclusion criteria: patients presenting with radiologically suspected glioblastoma were included. Gliomas analyzed were sourced from patients of varying demographics who underwent neurosurgical procedures at Greifswald University Medical Center with later validation as WHO \circ IV GBM by the in-house Institute of Pathology. Tumor localization was precisely accomplished using neuronavigation, defining six distinct areas: lateral, medial, ventral, dorsal, cranial, and caudal. Depending on tumor operability, three to five samples per patient were extracted from these defined regions, exclusively from the vital tumor margin, excluding necrotic-cystic central areas. Tumor samples, 5 mm in size, were embedded in a Tissue Tek Cryomold, snap-frozen in liquid nitrogen, and stored at -80°C . Subsequent cryostat sectioning yielded 5- μm -thick slices, with three sections per slide.

Acquisition of supernatants

Samples that were taken showed no signs of necrosis, no traces of electrocautery, hemostatic agents, or heavy blood deposits macroscopically. The degree of hemorrhage did not exceed normal tumor samples. Punched tissue samples were thoroughly washed in excess PBS to remove any remaining blood or serum prior to their short-term culture. Portions of the 5 mm tumor samples from each patient underwent initial incubation in 24-well plates containing culture medium (RPMI1640 supplemented with 2% penicillin/streptomycin; Thermo Fisher Scientific, Germany) at 37°C for 24 h. Post-incubation, the tumor samples were extracted from the medium and subjected to the previously described freezing process. In each instance, 1 ml of the resulting liquid supernatants underwent transfer to reaction tubes (Eppendorf, Germany), followed by centrifugation at 1,000 G for 2 min. Subsequently, 2 \times 200 μl aliquots from each Eppendorf tube were pipetted into separate wells of a 96-well round bottom plate. The resultant tissue-culture supernatants within the 96-well plates were then frozen at -80°C pending further measurement.

Immunofluorescence and imaging

After allowing the slides stored at -80°C to thaw for approximately 10 min at room temperature, sections were fixed with ice-cold (-20°C) acetone for 5 min, followed by four washing steps: a single rinse in phosphate-buffered saline (PBS) and three 5-min washes in PBS. The slides were gently tapped for drying and subsequent permeabilization with 50 μl 0.25% Triton-X100 solution for 2 min to enhance antibody or DAPI nuclear dye permeability. Following repeated rinsing and two 5-min washes, the slides were carefully dried. Antibody solutions, prepared

Table 1. Antibodies used in this study.

Antibody	Vendor	Catalog #	Host species
Arg-1	Abcam	Ab211961	Rabbit
CCR7	Novus Biologicals	NBP2 -31,089	Rabbit
CSFR-1	Abcam	Ab183316	Rabbit
CD16	BioRad	ABIN2478680	Rat
CD68	Abcam	Ab955	Mouse
CD163	Novus Biologicals	NBP1 -30,148	Rabbit
CD204	Novus Biologicals	NBP1 -88,125	Rabbit
CD206	Novus Biologicals	H00004360-M02	Mouse
GFAP	Invitrogen	13-0300	Rat
iNOS	Novus Biologicals	MAB9502	Mouse
MHC II	BioRad	MCA71R	Rat
PSGL-1	R&D Systems	MAB9961	Mouse
secondary antibody Alexa fluor 488	Thermo Fisher	A32723	Goat
secondary antibody Alexa fluor 597	Abcam	150160	Goat
secondary antibody Alexa fluor 647	Thermo Fisher	A32733	Goat

in 1% BSA, utilized 200 ng of each antibody per staining (Table 1). Slides were rimmed with a hydrophobic pen, and 50 μ l of the antibody solution was pipetted per section, incubating at 4°C overnight. Secondary antibody solutions contained a 1:1 mixture of 1% BSA and 10 μ M DAPI. After drying, 50 μ l of the secondary antibody solution was pipetted per section, incubating for 1 hour at room temperature, followed by several washing steps. The final step involved pipetting Fluor mount medium onto the slide, with subsequent measurement, imaging, and analysis conducted using a high-content imaging device (Operetta CLS; PerkinElmer, Germany) and associated software (Harmony 4.9, PerkinElmer, Germany).

Quenching background fluorescence

Untreated mouse brains were utilized for autofluorescence measurement, following the described sample treatment procedure. To assess the impact of tissue fixation on background fluorescence, two common fixatives, 4% PFA and acetone, were compared (Table 2). Mouse brains, post-surgical removal, were fixed for 24 h with 1 ml of either 4% PFA or acetone in a 1.7 ml reaction tube, followed by 24 h of dehydration in 30% sucrose solution at 4°C. The brains were then embedded in Tissue Tek and frozen in liquid nitrogen, stored at -80°C. Treatments with Sudan Black B (SBB) and controls with PBS were prepared for each fixative. SBB treatment involved pipetting at approximately 100 μ l per section, incubated in a humidity chamber for 20 min at room temperature. Subsequently, 50 μ l of a 10 μ M DAPI solution was pipetted onto two sections, incubated for 15 min in the dark at room temperature, and a final 10-min wash completed the staining. Slides were covered with fluor mount medium and a coverslip.

Analysis and quantification

Image analysis utilized Harmony 4.9 software (PerkinElmer, Germany), adapting the analysis approach for glioblastoma samples that exhibited significant variations in section characteristics and staining across patients. To standardize slice sizes, individual channels (DAPI, AF488, AF594, AF647) were normalized to the mean and smoothed. Subsequent segmentation of tissue sections based on intensity differences (red) was performed, defining cell nuclei via the DAPI channel. Agglomerations of nuclei deemed excessively large or contiguous were excluded, and initially, contiguous nuclei were appropriately split. Fluorescence intensities of antigen staining were determined by defining a region around the cell nucleus, incorporating an outward and inward ring for membrane-associated staining.^{31,32} The median, mean, sum, and standard deviation of fluorescence intensities within the ring region were quantified for each fluorescence channel (AF488, AF594, AF647). A distinct formula (Equation 1) was applied to create a heat map after obtaining analysis endpoints.

$$x = \frac{\text{Sum MFI} * n^{\text{positive cells}}}{\text{tissue area}} \quad (1)$$

Median fluorescence intensities (MFI) were selected for quantitative antigen expression representation due to their resistance to outliers. Positive staining was normalized to negative controls. Fold-change values for each area were summed for each marker across all 42 samples. Intratumoral heterogeneity investigation involved a normalization and scoring method. MFI values of antigens were aligned with their negative controls through subtraction, followed by normalization across all patient areas through division (Equation 2). Subtraction yielding negative results set values above the fraction line to “1,” indicating limited or negligible marker expression. For x values less than 1, another formula (Equation 3) was applied to calculate the heterogeneity score, which, in general,

Table 2. Acquisition settings at the operetta CLS high-content imaging device used in this study.

Acquisition channel	λ_{ex} (nm)	Exposure time (ms)	Diode power
DAPI	365	10	10%
Alexa fluor 488	475	50	50%
Alexa fluor 594	550	50	50%
Alexa fluor 647	630	50	40%
Brightfield	785	40	20%

is a score based on data from quantitative algorithm-driven image analysis of hundreds of tissue sections in contrast to most other published scores being based on subjective but blinded evaluator assessment. Conversely, x values exceeding 1 were directly multiplied by 100, denoting enhanced marker expression. Values within ± 150 received 5 heterogeneity points, while those exceeding the threshold were assigned 10 heterogeneity points, facilitating nuanced quantification of expression variations within the tumor.

$$x = \frac{MFI^{stain} - MFI^{control}}{\bar{x} * (MFI^{stain} - MFI^{control})} \quad (2)$$

$$Score = 0 - \left(\frac{1}{x < 1} \right) * 100 \quad (3)$$

Chemokine, cytokine, and growth factor quantification

Multiplex chemokine/cytokine analysis utilized a bead-based assay (BioLegend, The Netherlands) following the vendor's guidelines. Briefly, glioblastoma biopsy supernatants were incubated with beads, and mean fluorescence intensities (MFI) of each bead population, representing a single analyte, were determined through flow cytometry (CytoFLEX S; Beckman-Coulter, Germany). Total chemokine/cytokine concentrations were calculated against a known standard, employing 5-log fitting with dedicated software (VigeneTech, USA).

Statistical analysis

Graphs and statistical analyses were conducted using Prism 8.3 (GraphPad Software, USA). All values are displayed as mean \pm standard error of mean (SEM) or standard variation (SD) if not stated otherwise. The strength of the linear relationship between the two variables was calculated utilizing Pearson's correlation. Moreover, principal component analysis was used to show distinct differences between variables.

Results

Study procedures

The objective of this study was to investigate the intratumoral heterogeneity of macrophage- and tissue markers within gliomas. Punch biopsies were obtained from six distinct locations (lateral, medial, dorsal, ventral, caudal, cranial) during operative dissection (Figure 1a). A portion of the samples was incubated in cell culture medium for subsequent quantification of multiple cytokines through flow cytometry (Figure 1b). Another segment was embedded in cryo-medium and frozen for later sectioning, followed by high-content imaging with algorithm-based image quantification (Figure 1c).

Subsequent to this protocol, tissue slides underwent automated microscopic examination in various fields of view (FOV). The tissue was reconstructed with signals in up to four fluorescence channels employing diverse stainings

(Figure 1d 1–2). Pseudo-channels were generated using software algorithms, and morphological analysis tools were applied to modify them, facilitating software detection of the tissue region (Figure 1e 3–5). Automated software detection of nuclei and the perinuclear region allowed standardized and independent quantification of various markers, along with the calculation of distinct image properties (Figure 1e 6–9).

Different basal expression values of macrophage markers and cytokines in glioma samples

Examining the expression of macrophage- and tissue-markers in glioma samples revealed diverse basal levels. The fold change in staining intensity compared to the respective background varied, with values of 2.2 for Arg1, 3.2 for CCR7, 1.4 for CD16, 1.3 for CD68, 2.5 for CD163, 3.1 for CD204, 1.5 for CD206, 2.2 for CSF1R, 6.9 for GFAP (highest expression intensity), 2.7 for iNOS, 1.2 for MHC-II, and 1.5 for PSGL-1 (Figure 2a). Alternatively, expressing marker-positive cells per tissue area, an average of 1091 Arg1⁺ cells per mm² was observed, with CCR7 at 1401, CD16 at 386, CD68 at 587, CD163 at 458, CD204 at 1336, CD206 at 520, CSF1R at 971, GFAP at 1538, iNOS at 1088, MHC-II at 328, and PSGL-1 at 457 positive cells per mm² (Figure 2b).

Distinct cytokine levels in the supernatant of glioma biopsies varied among patients, with averages of 18.2 pg/ml for BDNF, 10.3 for β NGF, 488.9 for CCL2, 2530.9 for IL-6, 12.9 for IL-18, 63.0 for sTREM2, 4.4 for TGF β , 2.2 for TNF α , 2.3 for TREM1, 1114.3 for VEGF, and 31.2 pg/ml for VILIP-1 (Figure 2c). Consistently observed across all samples was the heterogeneity of marker distribution within the biopsies which was visualized through the multi-color staining approach (Figure 2d). Consequently, the next step involved investigating the heterogeneity of marker expression in biopsies from different glioma locations.

Intratumoral tissue-marker heterogeneity

As demonstrated earlier, various macrophage markers exhibit diverse expression intensities. Notable variations are evident among different patients and within distinct locations within a glioma (Figure 3a). The calculation of a heterogeneity score further underscores the variability of Arg-1, CCR7, CD16, CD18, CD68, CD163, CD204, CD206, CSF1R, GFAP, iNOS, MHC-II, and PSGL-1 expressions among patients and biopsy locations (colorized) (Figure 3b). CD16 displays the highest intratumoral heterogeneity among all markers, followed by PSGL-1, MHC-II, CD68, CD206, CD163, CSF1R, CD204, CCR7, iNOS, Arg1, and GFAP, with the lowest variation observed in GFAP (Figure 3c).

This heterogeneity is visually evident, with CD68 exhibiting a palisade-like or diffuse distribution in different locations within the same glioma (Figure 3d). CD163 is found distributed diffusely or around glioma vessels (Figure 3e). At the same time, CD204 shows varying cell densities across different biopsy locations (Figure 3f). GFAP exhibits differential

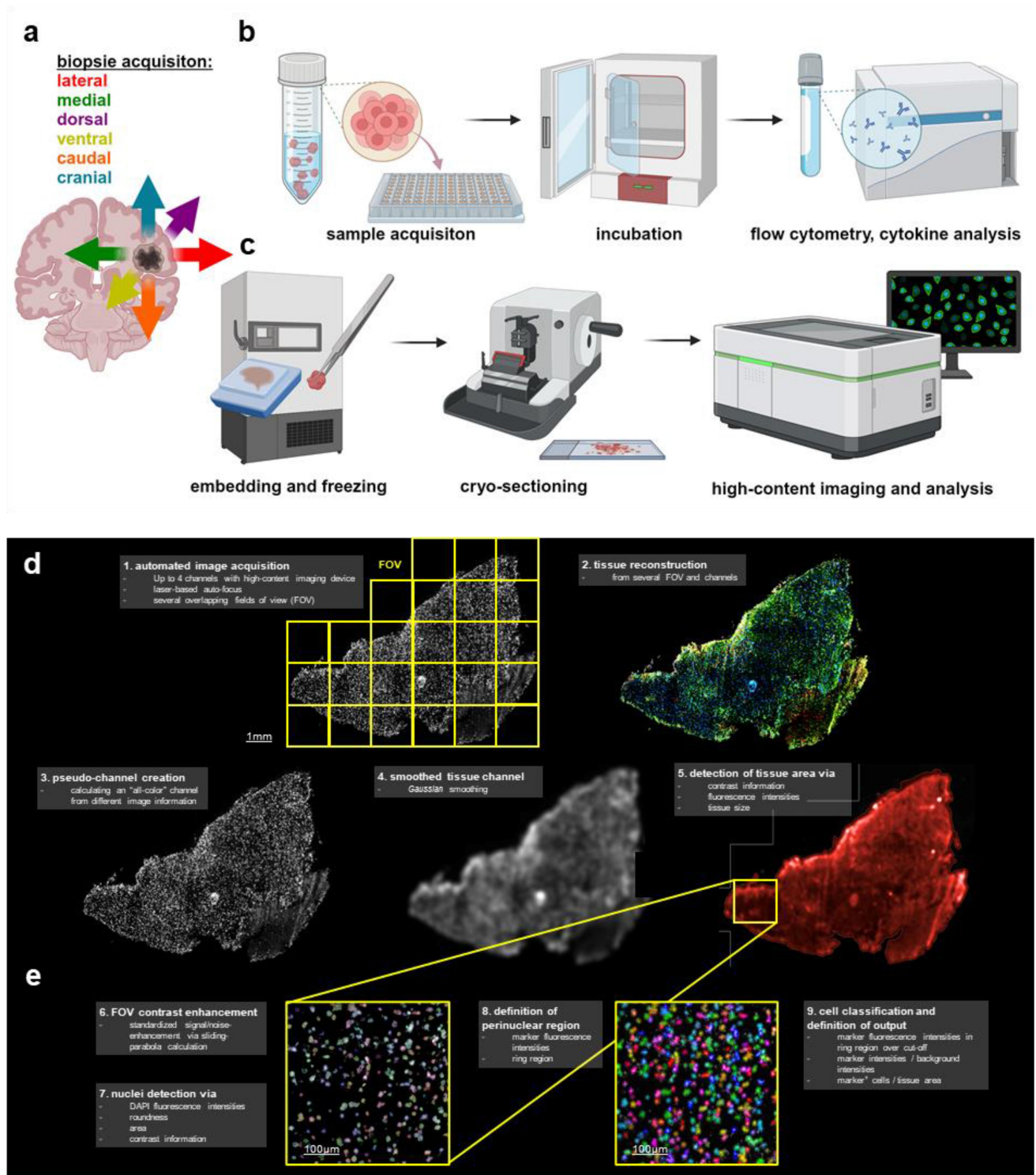


Figure 1. Schematic overview of study procedures and image quantification workflow. (a) information about local positions of lateral, medial, dorsal, ventral, caudal, and cranial biopsies; (b) temporary storage of punch-biopsy samples sample tubes before they were transferred to cell-culture plates and incubated, following flow cytometry for cytokine analysis in the biopsies supernatant; (c) embedding of other biopsy samples and shock freezing at -80°C , cryo-sectioning and multi-color fluorescence staining and analysis via high-content image cytometry and algorithm-based image quantification; (d) automated image acquisition in several fields of view (FOV), tissue reconstruction out of different fluorescence channels, calculation of a pseudo image, image smoothing, and detection of the tissue region; (e) contrast enhancement and nuclei detection in every field of view inside the tissue region, definition of perinuclear region, and calculation of marker fluorescence and morphological values inside the different regions.

expression, appearing associated with cell density (Figure 3g). PSGL-1, characterized by high intratumoral heterogeneity, is observed in varying densities and vessel-like structures

(Figure 3h). Reassessing the staining over background for PSGL-1 reveals distinct intensities between locations and patients (Figure 3i).

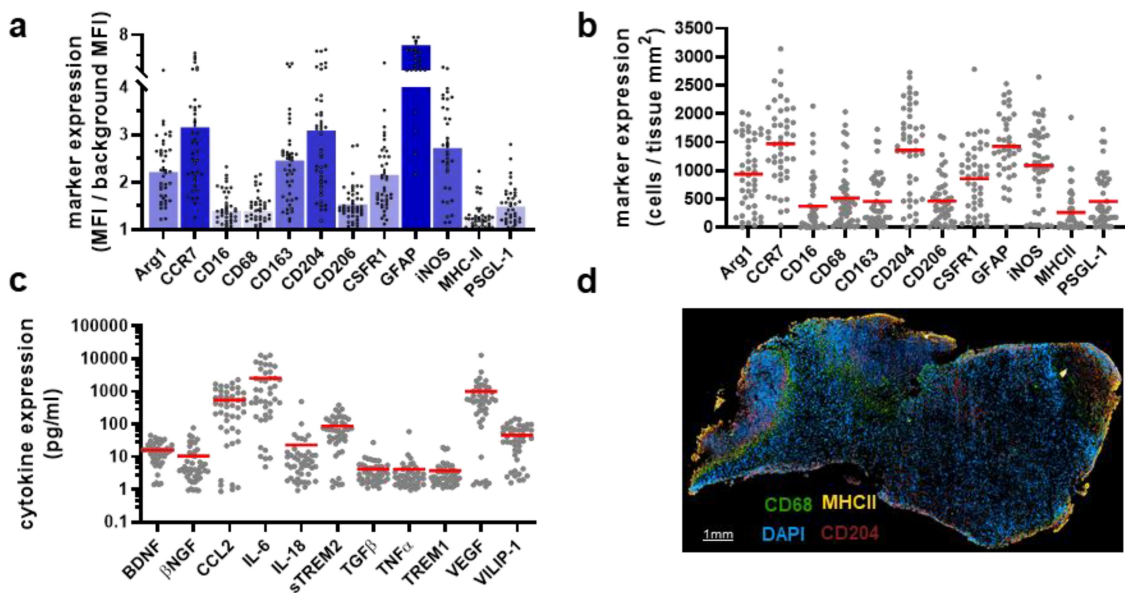


Figure 2. Marker- and cytokine-expression. (a) expression of tissue markers (Arg1, CCR7, CD68, CD163, CD204, CD206, CSFR1, GFAP, iNOS, MHC-II, PSGL-1) compared to their distinct background as analyzed using high-content imaging; (b) expression of tissue markers as marker-positive cells per mm² of tissue area as analyzed using high-content imaging; (c) cytokine expression (BDNF, β NGF, CCL2, IL-6, sTREM2, TGF β , TNF α , TREM1, VEGF, VILIP-1) in pg/ml measured in biopsy supernatant as analyzed by multi-color flow cytometry.

Intratumoral cytokine heterogeneity

Consistent patterns of heterogeneous expressions were observed not only among patients but also in the supernatants from different biopsy locations for cytokines in the samples (Figure 4a). Computation of a heterogeneity score revealed that β NGF exhibited the highest variation among the different biopsy locations, followed by IL-6, IL-18, TNF α , CCL2, VEGF, VILIP-1, TREM1, TGF β , sTREM2, and with the lowest heterogeneity, BDNF (Figure 4b).

Several cytokines demonstrated interdependence, indicating coordinated regulation. The cytokine secretion in the biopsies exhibited correlated heterogeneity (Figure 4c). Of note, a range of markers and cytokines showed significant correlation with some or several surface or secretion molecules (Table 3). Employing principal component analysis to identify the cytokine contributing most to the heterogeneity, VILIP-1 emerged as distinctive from other cytokines, with CCL2, CD163, and CD204 showing opposing tendencies, and IL-18 displaying the highest similarities (Figure 4d). Noteworthy variations were also found among the expression of TREM1, β NGF, and TGF β compared to sTREM2, MHC-II, and CD206 for the remaining cytokines (Figure 4d). In addition, especially CD204, CCL2, and PSGL-1 significantly (Figure 4e) and mostly positively (Figure 4c) correlated with the release and expression of many studied molecules, which was not case especially for IL-18, TNF α , and VILIP-1 showing only 1–2 significant correlations to other markers studied.

Discussion

In this study, the intratumoral heterogeneity of tumor-associated macrophages (TAM) and microglial cells in human glioblastoma (GBM) tissue was investigated. Research into intratumoral heterogeneity has gained importance over

the last decade, with the large-scale molecular genetic sequencing of over 200 tumors in the “Cancer Genome Atlas Research Network” as one of its milestones.³³ Subsequently, the four most common GBM subtypes gain relevance through different therapy approaches.^{34–36} As the largest non-neoplastic cell population in GBM, with about 40%, TAM is an important component of the tumor microenvironment.³⁷ They comprise resident microglial cells and macrophages migrating from the blood.²² The heterogeneity of the macrophage phenotypes was historically differentiated in a very simplified way into an anti-tumor M1 and tumor-supportive M2 phenotype. RNA sequencing showed that in vivo, there is rather a dynamic mixed picture of these phenotypes, which means that the earlier classification seems outdated.²⁰ Therefore, the antigens investigated cover both anti-tumor and tumor-supportive TAM marker molecules. The composition and heterogeneity of different macrophage phenotypes have not been studied in different biopsy locations of the same tumor before. Still, the data from the present work show that highly expressed (macrophage) markers show low intratumoral heterogeneity among the different tumor areas. GFAP, the most strongly expressed marker investigated here, showed the lowest intratumoral heterogeneity. Thus, GFAP was expressed in the examined tumors with relatively small deviations, which is not surprising, because of its expression by the tumor cells itself as well as the high density of these cells.³⁸ Markers with a low measured total expression, which includes PSGL-1, CD16, CD68, and MHC-II, showed pronounced intratumoral heterogeneity. This could be related to the fact that several GBM subtypes can occur simultaneously within a tumor, but mostly the mesenchymal subtype is characterized by a high incidence of immune cells.^{39,40}

PSGL-1, one of the investigated markers, belonged to the group of the lowest expressed antigens alongside MHC-II, CD16, and CD68. PSGL-1 is known to be expressed in a wide

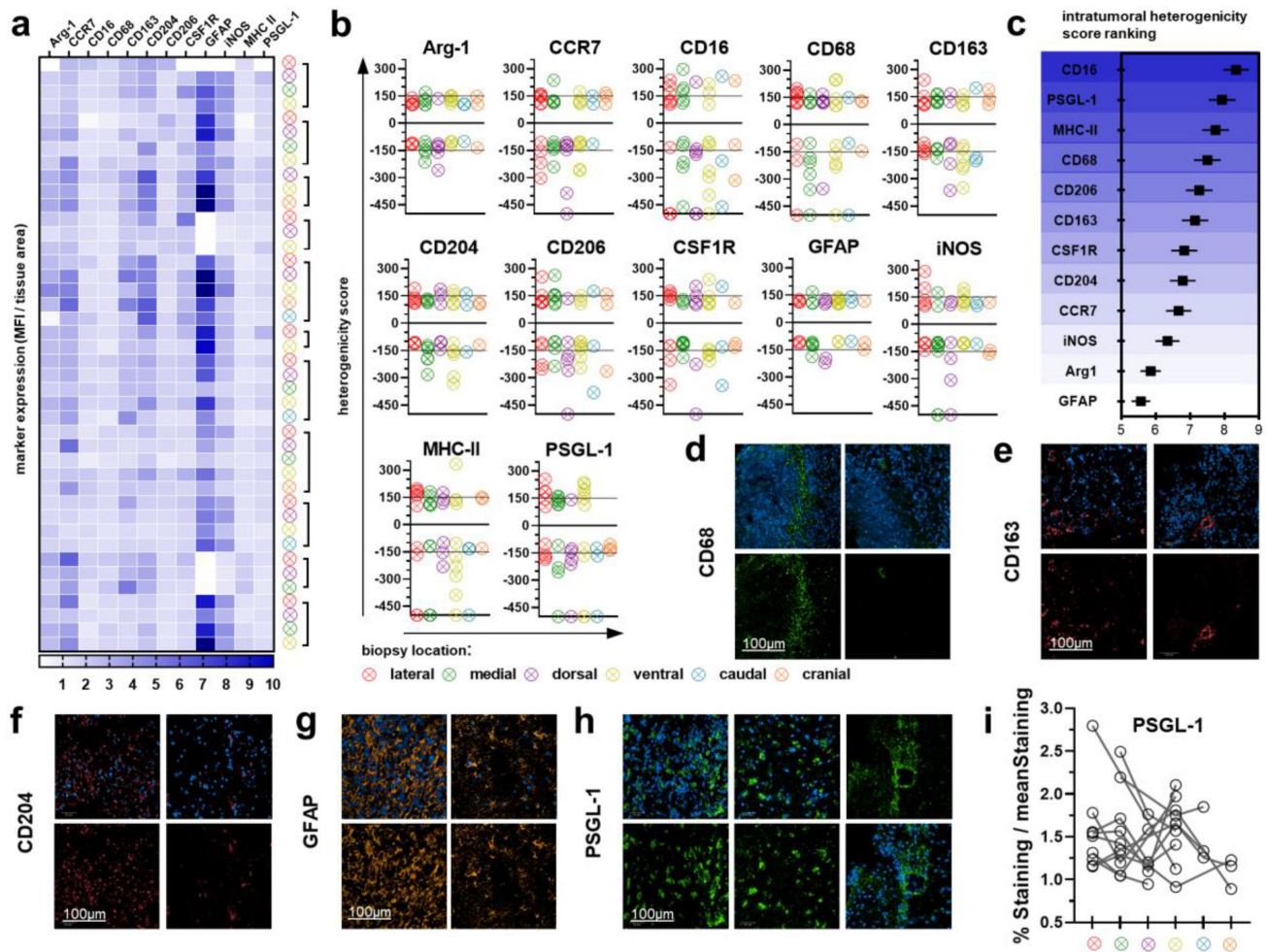


Figure 3. Intratumoral tissue-marker heterogeneity. (a) heat-map with the overview of different markers per biopsy location and per patient as analyzed using high-content imaging; (b) intratumoral heterogeneity score calculated for all tissue markers as analyzed using high-content imaging; (c) ranking of the average intratumoral heterogeneity score of all markers as analyzed using high-content imaging; (d) representative images of tissue in their DAPI (blue) and CD68 channels (green) for two different biopsy locations as analyzed using high-content imaging; (e) representative images of tissue in their DAPI (blue) and CD163 channels (red) for two different biopsy locations as analyzed using high-content imaging; (f) representative images of tissue in their DAPI (blue) and CD204 channels (red) for two different biopsy locations as analyzed using high-content imaging; (g) representative images of tissue in their DAPI (blue) and GFAP channels (orange) for two different biopsy locations as analyzed using high-content imaging; (h) representative images of tissue in their DAPI (blue) and PSGL-1 channels (green) for three different biopsy locations as analyzed using high-content imaging; (i) staining heterogeneity compared to the distinct mean-staining of PSGL-1 in different biopsy locations and different patients as analyzed using high-content imaging.

variety of cell types, including dendritic cells, CD4⁺ T cells, CD8⁺ T cells, neutrophils, regulatory T cells, hematopoietic stem cells, monocytes, and macrophages.^{41,42} PSGL-1-expressing cells can adhere to the endothelial surface by binding to P, L, or E selectins and finally migrate into the tissue.⁴³ Especially in glioma, the P-selectin expression can be increased, which leads to a more permeable BBB.⁴⁴ Other studies show that in Selp1g (PSGL-1 gene) knockout models, the leukocyte migration inside the brain is reduced.⁴⁵ Also, in our research, the PSGL-1⁺ cells were found mostly in cluster-like structures around the vessels. The expression density decreased with increasing distance from such vessel structures. In other studies, PSGL-1 is, therefore, also used as a semi-specific vascular marker in glioma tissue.⁴⁶ This is understandable since PSGL-1 binds directly to the selectins expressed on the endothelial to migrate. PSGL-1 is also involved in other crucial processes. For example, we previously found reduced platelet-monocyte formation in the circulation of GBM patients, although the

thrombocytes are highly activated.⁴⁷ A possible explanation for this is a decreased expression of PSGL-1 in the monocytes. Platelet-monocyte conjugates can convert circulating monocytes from an undefined- (CD14⁺/CD16⁻) to an anti-tumor phenotype (CD14⁺/CD16⁺).⁴⁸ The anti-tumor mode of action of PSGL-1 on myeloid cells and, thus, the putative explanation for the low expression in GBM patients appears conclusive since GBM is known for its immunosuppressive tumor microenvironment.^{49,50} However, current research on PSGL-1 on diverse immune cells shows a more heterogenic picture.^{42,51,52} The study by Yuan et al. (2024) reveals crucial insights into the expression patterns of immune checkpoints in glioblastoma (GBM) using single-nucleus RNA sequencing (snRNA-Seq) and spatial transcriptomics (ST). The researchers identified a prominent expression of TIM-3, VISTA, PSGL-1, and VSIG-3 in GBM, suggesting their potential as therapeutic targets. Additionally, high VISTA expression was linked to poorer prognosis, emphasizing the complexity of the GBM

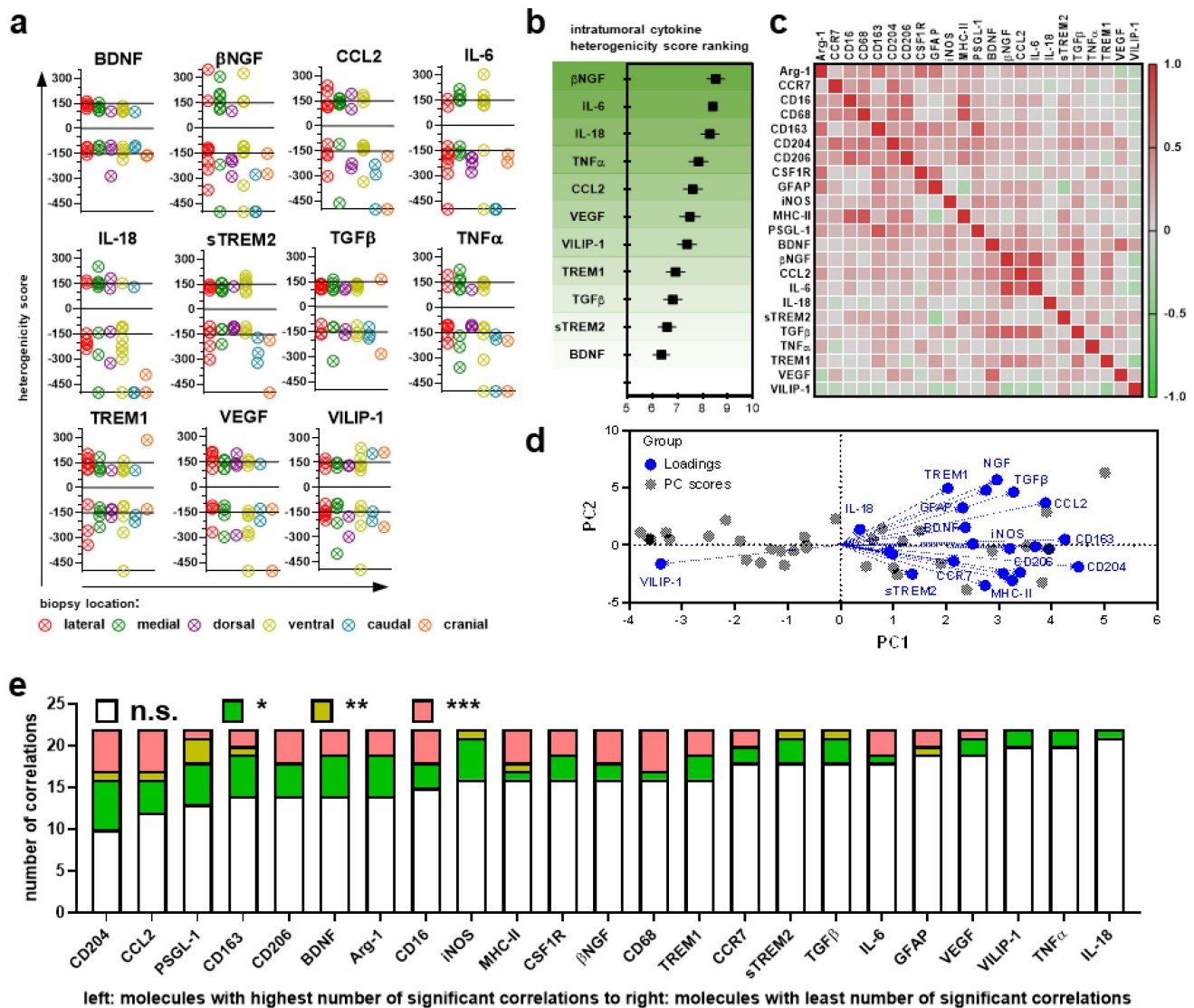


Figure 4. Intratumoral cytokine heterogeneity. (a) intratumoral heterogeneity of cytokines in the supernatant of tumor biopsies as analyzed using multi-color flow cytometry; (b) intratumoral heterogeneity score of cytokines in the supernatant of tumor biopsies as analyzed using multi-color flow cytometry; (c) heat-map with the overview of the correlation of the different cytokines as analyzed using multi-color flow cytometry and cell surface markers as analyzed using high-content imaging; (d) principal component analysis showing the impact of different cytokines in creating intratumoral heterogeneity; (e) waterfall-plot of cumulative numbers of significant Pearson correlations of a given marker with all other markers of that plot (see Table 3 for details) indicating CD204 and CCL2 to be associated the most and IL-18 and TNF α to be associated the least with any tissue or secretion target quantitative analyzed in this study.

tumor microenvironment and its intracellular communication networks. PSGL-1's role in immune modulation within the tumor microenvironment is underscored by its involvement in crucial interactions with selectins, facilitating immune cell migration and potentially contributing to immune evasion mechanisms. The co-expression of PSGL-1 with other immune checkpoints like VISTA and TIM-3 reinforces its relevance in the immunosuppressive landscape of GBM, making it a significant marker for understanding and targeting GBM's complex biology.⁵³

Besides GFAP, the anti-tumor CCR7⁵⁴ showed the strongest expression among the investigated markers. Other studies show that a high CCR7 expression in GBM can increase the invasiveness of tumor cells via TGF β 1 and the NF κ B signaling pathway.⁵⁵ However, we did not find TGF β 1 to be a predominant cytokine in our samples. The investigated markers that are rather associated with an anti-tumor phenotype

are CD16, CD68, iNOS, and MHC-II.^{56–59} On the other hand, iNOS was found to increase proliferation and lower survival when expressed on CD133⁺ tumor stem cells.⁶⁰ CD16 on monocytes, macrophages, or NK cells was not detailedly investigated in GBM before.⁶¹ We conclude that macrophages are responsible for the detected low amount of CD16, which was rather located inside the tissue than surrounding the blood vessels. In this study's stainings, we found a high density of CD68⁺ and CD163⁺ cells. While CD163⁵⁹ is rather functioning as a pan-TAM marker,^{62,63} CD68 is more associated with an activation status. In the acquired images, a pseudopalisade arrangement of CD68⁺ stained tumor cells can be seen around a necrotic area, a typical histopathological characteristic of GBM.⁷ Consistently, CD204 is expressed within the necrotic area since CD204-expressing cells, as members of the scavenger receptor family, can bind and internalize ligands, including apoptotic cells, modified molecules, and myelin.⁶⁴ MHC-II was

Table 3. Pearson r statistical correlation table showing p-values for each comparison that have been marked for better overview (green = p < 0.05; yellow = p < 0.01; red = p < 0.001).

	Arg-1	CCR7	CD16	CD68	CD163	CD204	CD206	CSF1R	GFAP	iNOS	MHC-II	PSGL-1	BDNF	βNGF	CCL2	IL-6	IL-18	sTREM2	TGFB	TNFα	TREM1	VEGF	VILIP-1	
Arg-1																								
CCR7	0.5814																							
CD16	0.0199	0.0332																						
CD68	0.0514	0.0010	0.0002																					
CD163	0.0000	0.8548	0.0717	0.1520																				
CD204	0.0620	0.0000	0.0007	0.0000	0.0220																			
CD206	0.0462	0.0345	0.0000	0.0001	0.0179	0.0001																		
CSF1R	0.0000	0.7945	0.4341	0.9697	0.0001	0.0233	0.1312																	
GFAP	0.0005	0.2487	0.8200	0.8149	0.0037	0.1715	0.3512	0.0009																
iNOS	0.4397	0.2993	0.3144	0.2427	0.0137	0.0535	0.0873	0.8032	0.8846															
MHC-II	0.0347	0.0620	0.0000	0.0000	0.2792	0.0009	0.0003	0.8787	0.1182	0.5934														
PSGL-1	0.0166	0.2763	0.1030	0.0438	0.0000	0.0019	0.0106	0.0227	0.1611	0.0032	0.3531													
BDNF	0.8433	0.8071	0.5316	0.4913	0.1518	0.0239	0.1956	0.7349	0.3438	0.0196	0.3787	0.2464												
βNGF	0.2278	0.6756	0.2740	0.8369	0.0693	0.1866	0.5405	0.6278	0.0697	0.1512	0.3787	0.2464	0.0252											
CCL2	0.0156	0.7727	0.0456	0.2101	0.0213	0.1270	0.0525	0.6508	0.0876	0.0116	0.0252	0.1787	0.0050	0.0009	0.0000	0.0000	0.0000	0.0000	0.0000	0.0000	0.0000	0.0000	0.0000	0.0000
IL-6	0.4052	0.8738	0.1117	0.9570	0.2018	0.5728	0.2431	0.5643	0.1477	0.2005	0.9400	0.3164	0.0050	0.0000	0.0000	0.0000	0.0000	0.0000	0.0000	0.0000	0.0000	0.0000	0.0000	0.0000
IL-18	0.4063	0.5659	0.9394	0.6166	0.8462	0.4108	0.6621	0.2390	0.8902	0.9523	0.7756	0.7362	0.2456	0.1787	0.0252	0.0000	0.0000	0.0000	0.0000	0.0000	0.0000	0.0000	0.0000	0.0000
sTREM2	0.5503	0.9519	0.1125	0.0716	0.1254	0.0437	0.2318	0.2686	0.0789	0.1512	0.7362	0.2456	0.1787	0.0252	0.0000	0.0000	0.0000	0.0000	0.0000	0.0000	0.0000	0.0000	0.0000	0.0000
TGFB	0.4263	0.3132	0.6119	0.4974	0.0745	0.0128	0.6024	0.9545	0.0876	0.0116	0.0252	0.1787	0.0050	0.0000	0.0000	0.0000	0.0000	0.0000	0.0000	0.0000	0.0000	0.0000	0.0000	0.0000
TNFα	0.1112	0.4737	0.9285	0.8022	0.1418	0.1698	0.8188	0.0455	0.7381	0.0176	0.7661	0.0498	0.0001	0.0000	0.0000	0.0000	0.0000	0.0000	0.0000	0.0000	0.0000	0.0000	0.0000	0.0000
TREM1	0.5155	0.9895	0.9340	0.9610	0.0358	0.4866	0.4206	0.6760	0.0541	0.4438	0.8436	0.0714	0.0904	0.0003	0.0000	0.0000	0.0000	0.0000	0.0000	0.0000	0.0000	0.0000	0.0000	0.0000
VEGF	0.1535	0.1657	0.6297	0.6701	0.8930	0.0215	0.1451	0.6366	0.5716	0.0435	0.9799	0.8292	0.0000	0.9697	0.9206	0.1345	0.1080	0.1080	0.1080	0.1080	0.1080	0.1080	0.1080	0.1080
VILIP-1	0.3070	0.3217	0.7006	0.4438	0.5605	0.9216	0.6889	0.6858	0.3216	0.2482	0.7831	0.5923	0.0376	0.0917	0.3428	0.1047	0.8826	0.1446	0.5212	0.8188	0.0298	0.3262	0.3262	

found to be expressed low and with a high heterogeneity. This is also described by other studies investigating GBM with a higher expression after immunostimulation.^{65,66} In another study, MHC-II and CD204 were coexpressed on average in 44% (range: 3% to 85%) of the cells, which suggests that the macrophages are subject to a certain dynamic in the phenotype.⁴⁶ Also, CD204 was described as very heterogeneously distributed inside the tumor, with an overall high expression lowering the survival.⁴⁶ Other investigated tumor-supportive macrophage markers include Arg1, CD163, CD206, and CSF1R.^{54,67,68} The CD206-expressing tumor-supportive phenotype can be induced via IL6,⁶⁹ which was found to be increased in our samples, but the other markers showed higher expression levels in the measured samples. Also, CD163 can be induced in monocytes, which can be increased in the context of tumor-supportive GBM.⁵⁴ Another example of the importance of investigating intratumoral heterogeneity is CSF1R. The expression of this receptor correlates with a poor prognosis in various tumor types,⁷⁰ but attempts of CSF1R inhibitors failed in the GBM.⁶⁸ The explanation could be that only a partial tumor fraction is hit by such therapies because (as found in this study) the receptor is expressed very variable.

Besides the rather static surface antigen, we investigated the heterogeneity of several cytokines. We found high basal expression levels for the pro-inflammatory IL-6,⁷¹ while other pro-inflammatory markers, such as TNF α ,⁷² were measured in low quantities. This could be explained by a lack of non-classical and TNF α -producing monocytes,⁷³ which were also not found in large quantities here. For IL-6, a high heterogeneity was measured, so it can be concluded that this depends on the tumor status or cell density and that it will also function as an anti-inflammatory cytokine in GBM.⁶³ In other multiplex analyses, it was shown that numerous cytokines, including CCL-2, are highly expressed in the inflammatory milieu of rapidly progressive GBM. This is due to glioma cell-host cell interactions.⁷⁴ In this study, CCL-2 was one of the most highly expressed cytokines, along with IL-6 and VEGF. CCL-2 can be considered a parameter for increased TAM recruitment/invasion.⁷⁵ Another regulator is IL-13, which can increase the CCL-2 expression (as measured here), as well as induce the P2ry13 and Selp1g gene, which codes for PSGL-1.⁷⁴ These findings could be another explanation for the high intratumoral PSGL-1 heterogeneity. All in all, the complex microglia populations seem to be an important driver for cytokine heterogeneity. VILIP-1, another of the tested cytokines, appears to be of outstanding importance since it was the greatest determinant, dividing it from the other markers in the principle-component analysis. VILIP-1 functions as a neuronal calcium sensor, as well as over cGMP-signaling, and is involved especially in neurodegenerative diseases such as Alzheimer's disease.^{76,77} The relevance of its expression in GBM has not been studied in detail yet, but recent studies suggest calcium sensing to be crucial for GBM networking and tumor progression.⁷⁸ However, different tumor types as squamous cell carcinoma or lung carcinoma, it is known to increase the tumor cell migration and to lower the overall survival.^{79,80} The potential effect in this study could be altered neuronal signaling in GBM tissue or neurodegenerative processes, which were measured and are not in direct relation with the tumor disease.

In this study, most of the markers that were detected to be elevated represent a more immunosuppressive TME^{20,50} with a complex heterogeneity. However, the TAM can often represent both geno-²⁵ or phenotypes.^{46,74} Around 85% of TAM migrate via the bloodstream, with only the rest being resident macrophages (microglia). The perivascular marker expression played an important role.¹⁹ The polarization in M1 and M2 phenotypes is not stable but rather a dynamic process,¹ which fits perfectly in the highly measured heterogeneity within the tumor samples. The same applies to the tumor cells themselves that were shown in other studies to have heterogenic phenotypes at a single-cell level within one sample.⁴⁰ Also, when comparing the tumor margins with the center, similar effects could be described for the tumor cells themselves.⁸¹

In summary, our findings highlight the complex and heterogeneous nature of the GBM microenvironment, with TAMs and microglial cells exhibiting diverse phenotypes and roles. Further research is needed to understand the spatial distribution and functional implications of these cells within different tumor regions, such as perivascular, hypoxic/necrotic, and invasive zones. Future work will also focus on distinguishing the contributions of tumor-associated macrophages versus resident microglia to better understand their respective roles in GBM heterogeneity and progression.

Study limitations

Intratumoral heterogeneity in glioblastoma complicates patient comparisons due to variable tumor locations and inconsistent sample extraction areas. Immunofluorescence on frozen sections offers limited tissue morphology assessment and suffers from brain tissue autofluorescence, which acetone fixation can reduce, though it may alter staining patterns. The study faced constraints with co-expression analysis, as only up to three antigens could be stained and imaged simultaneously, requiring multiple serial sections and complicating exact localization. Identifying whether antigens were expressed by immune or tumor cells was challenging, and no glioma-specific stem cell marker exists. Hence, our study did not attempt to define distinct (immune) cell populations, as their unambiguous identification in tissue sections would require single-cell gene expression analysis (spatial transcriptomics), which could not be realized in our study. Moreover, statistical analysis of intratumoral heterogeneity was infeasible due to the lack of comparable biological (healthy) samples and vascular markers, limiting insights into the relationship between antigen expression and tissue vascularization.

Conclusion

In conclusion, this study investigated the intratumoral heterogeneity of important TAM markers in different biopsy locations of human GBM. TAM, constituting the largest non-neoplastic cell population in GBM, plays a crucial role in the TME. The study revealed that highly expressed macrophage markers showed low intratumoral heterogeneity among different tumor areas, with GFAP, the most strongly expressed marker, displaying the lowest heterogeneity. Conversely, markers with low total expression, such as PSGL-1, CD16, CD68, and MHC-II, exhibited pronounced intratumoral heterogeneity, possibly reflecting the

coexistence of different GBM subtypes within a tumor. Detailed analysis of PSGL-1, a marker associated with cell migration, revealed its heterogeneous distribution, particularly around vessels, suggesting its potential role as a marker for vascular monocyte migration. The complex functions of PSGL-1, including its involvement in immunosuppressive processes, present challenges in understanding its role in the immune environment of GBM. Markers associated with anti-tumor phenotypes, such as CCR7, CD16, CD68, iNOS, and MHC-II, showed varying levels of expression, emphasizing the dynamic nature of macrophage phenotypes within the tumor. Additionally, the study highlighted the heterogeneity in cytokine expression, with IL-6, CCL-2, and VEGF exhibiting high basal levels. In summary, this descriptive study shows the importance of investigating intratumoral heterogeneity in both macrophage markers and cytokines within GBM. The findings contribute valuable insights into the complex immune landscape of GBM, supporting the need for personalized treatment strategies, as well as the utilization of biopsies from more than one tumor location for reliable diagnostics.

Acknowledgments

The authors acknowledge technical support by Felix Niessner and Juliane Moritz (INP, Greifswald, Germany).

Disclosure statement

No potential conflict of interest was reported by the author(s).

Funding

This work was funded by the German Federal Ministry of Education and Research (BMBF), grant numbers [03Z22DN11 and 03Z22Di1] (to S.B.), the Gerhard-Domagk-Foundation and Liselotte-Beutel Foundation (to S.M.).

ORCID

Sander Bekeschus  <http://orcid.org/0000-0002-8773-8862>

Author contributions

Conceptualization, S.M. and S.B.; methodology, M.I., E.F., and S.B.; software, M.I., E.F., and S.B.; validation, M.I., S.M., E.F., and S.B.; formal analysis, M.I., S.M., and E.F.; investigation, M.I., E.F., and S.B.; resources, K.R., H.W.S.S., and S.B.; data curation, S.M., K.R., H.W.S.S., and S.B. writing – original draft preparation, S.B. and M.I.; visualization, E.F.; supervision, S.M., and S.B.; project administration, S.B.; funding acquisition, S.B. All authors have read and agreed to the published version of the manuscript.

Data availability statement

Data are available from the corresponding authors upon reasonable request.

Informed consent statement

Informed consent was obtained from all subjects involved in the study.

Institutional review board statement

The study was conducted in accordance with the Declaration of Helsinki and approved by the Institutional Ethics Committee of the Greifswald University Medical Center (Germany, protocol code BB089/08b).

References

- Vitale I, Shema E, Loi S, Galluzzi L. Intratumoral heterogeneity in cancer progression and response to immunotherapy. *Nat Med.* 2021;27(2):212–224. doi:10.1038/s41591-021-01233-9.
- Xiong Z, Yang Q, Li X. Effect of intra- and inter-tumoral heterogeneity on molecular characteristics of primary idh-wild type glioblastoma revealed by single-cell analysis. *CNS Neurosci Ther.* 2020;26(9):981–989. doi:10.1111/cns.13396.
- Davis FG, Smith TR, Gittleman HR, Ostrom QT, Kruchko C, Barnholtz-Sloan JS. Glioblastoma incidence rate trends in Canada and the United States compared with England, 1995–2015. *Neuro Oncol.* 2020;22(2):301–302. doi:10.1093/neuonc/noz203.
- Ohgaki H, Kleihues P. Epidemiology and etiology of gliomas. *Acta Neuropathol.* 2005;109(1):93–108. doi:10.1007/s00401-005-0991-y.
- Pombo Antunes AR, Scheyltjens I, Lodi F, Messiaen J, Antoranz A, Duerinck J, Kancheva D, Martens L, De Vlaminck K, Van Hove H. et al. Single-cell profiling of myeloid cells in glioblastoma across species and disease stage reveals macrophage competition and specialization. *Nat Neurosci.* 2021;24(4):595–610. doi:10.1038/s41593-020-00789-y.
- Louis DN, Wesseling P, Aldape K, Brat DJ, Capper D, Cree IA, Eberhart C, Figarella-Branger D, Fouladi M, Fuller GN. et al. cIMPACT-now update 6: new entity and diagnostic principle recommendations of the cIMPACT-Utrecht meeting on future CNS tumor classification and grading. *Brain Pathol.* 2020;30(4):844–856. doi:10.1111/bpa.12832.
- Hambardzumyan D, Bergers G. Glioblastoma: defining tumor niches. *Trends Cancer.* 2015;1(4):252–265. doi:10.1016/j.trecan.2015.10.009.
- Couto M, Coelho-Santos V, Santos L, Fontes-Ribeiro C, Silva AP, Gomes CMF. The interplay between glioblastoma and microglia cells leads to endothelial cell monolayer dysfunction via the interleukin-6-induced JAK2/STAT3 pathway. *J Cell Physiol.* 2019;234(11):19750–19760. doi:10.1002/jcp.28575.
- Feng X, Szulzewsky F, Yerevanian A, Chen Z, Heinzmann D, Rasmussen RD, Alvarez-Garcia V, Kim Y, Wang B, Tamagno I. et al. Loss of CX3CR1 increases accumulation of inflammatory monocytes and promotes gliomagenesis. *Oncotarget.* 2015;6(17):15077–15094. doi:10.18632/oncotarget.3730.
- Wippold FJ 2nd, Lämmle M, Anatelli F, Lennerz J, Perry A. Neuropathology for the neuroradiologist: palisades and pseudopalisades. *AJNR Am J Neuroradiol.* 2006;27(10):2037–2041.
- Brat DJ, Van Meir EG. Vaso-occlusive and prothrombotic mechanisms associated with tumor hypoxia, necrosis, and accelerated growth in glioblastoma. *Lab Invest.* 2004;84(4):397–405. doi:10.1038/labinvest.3700070.
- Soeda A, Park M, Lee D, Mintz A, Androutsellis-Theotokis A, McKay RD, Engh J, Iwama T, Kunisada T, Kassam AB. et al. Hypoxia promotes expansion of the CD133-positive glioma stem cells through activation of HIF-1 α . *Oncogene.* 2009;28(45):3949–3959. doi:10.1038/onc.2009.252.
- Seidel S, Garvalov BK, Wirta V, von Stechow L, Schänzer A, Meletis K, Wolter M, Sommerlad D, Henze A-T, Nistér M. et al. A hypoxic niche regulates glioblastoma stem cells through hypoxia inducible factor 2 α . *Brain.* 2010;133(4):983–995. doi:10.1093/brain/awq042.
- Cuddapah VA, Robel S, Watkins S, Sontheimer H. A neurocentric perspective on glioma invasion. *Nat Rev Neurosci.* 2014;15(7):455–465. doi:10.1038/nrn3765.
- Westphal M, Lamszus K. The neurobiology of gliomas: from cell biology to the development of therapeutic approaches. *Nat Rev Neurosci.* 2011;12(9):495–508. doi:10.1038/nrn3060.

16. Watkins S, Robel S, Kimbrough IF, Robert SM, Ellis-Davies G, Sontheimer H. Disruption of astrocyte–vascular coupling and the blood–brain barrier by invading glioma cells. *Nat Commun.* 2014;5(1):4196. doi:10.1038/ncomms5196.
17. Charles NA, Holland EC, Gilbertson R, Glass R, Kettenmann H. The brain tumor microenvironment. *Glia.* 2012;60(3):502–514. doi:10.1002/glia.21264.
18. Chen Z, Feng X, Herting CJ, Garcia VA, Nie K, Pong WW, Rasmussen R, Dwivedi B, Seby S, Wolf SA. et al. Cellular and molecular identity of tumor-associated macrophages in glioblastoma. *Cancer Res.* 2017;77(9):2266–2278. doi:10.1158/0008-5472.CAN-16-2310.
19. Buonfiglioli A, Hambarzumyan D. Macrophages and microglia: the Cerberus of glioblastoma. *Acta Neuropathol Commun.* 2021;9(1):54. doi:10.1186/s40478-021-01156-z.
20. Chen Z, Hambarzumyan D. Immune microenvironment in glioblastoma subtypes. *Front Immunol.* 2018;9:1004. doi:10.3389/fimmu.2018.01004.
21. Ginhoux F, Greter M, Leboeuf M, Nandi S, See P, Gokhan S, Mehler MF, Conway SJ, Ng LG, Stanley ER. et al. Fate mapping analysis reveals that adult microglia derive from primitive macrophages. *Science.* 2010;330(6005):841–845. doi:10.1126/science.1194637.
22. Epelman S, Lavine KJ, Randolph GJ. Origin and functions of tissue macrophages. *Immunity.* 2014;41(1):21–35. doi:10.1016/j.immuni.2014.06.013.
23. Elmore MP, Najafi A, Koike M, Dagher N, Spangenberg E, Rice R, Kitazawa M, Matusow B, Nguyen H, West B. et al. Colony-stimulating factor 1 receptor signaling is necessary for microglia viability, unmasking a microglia progenitor cell in the adult brain. *Neuron.* 2014;82(2):380–397. doi:10.1016/j.neuron.2014.02.040.
24. Kettenmann H, Kirchhoff F, Verkhratsky A. Microglia: new roles for the synaptic stripper. *Neuron.* 2013;77(1):10–18. doi:10.1016/j.neuron.2012.12.023.
25. Muller S, Kohanbash G, Liu SJ, Alvarado B, Carrera D, Bhaduri A, Watchmaker PB, Yagnik G, Di Lullo E, Malatesta M. et al. Single-cell profiling of human gliomas reveals macrophage ontogeny as a basis for regional differences in macrophage activation in the tumor microenvironment. *Genome Biol.* 2017;18(1):234. doi:10.1186/s13059-017-1362-4.
26. Chen Z, Herting CJ, Ross JL, Gabanic B, Puigdelloses Vallcorba M, Szulzewsky F, Wojciechowicz ML, Cimino PJ, Ezhilarasan R, Sulman EP. et al. Genetic driver mutations introduced in identical cell-of-origin in murine glioblastoma reveal distinct immune landscapes but similar response to checkpoint blockade. *Glia.* 2020;68(10):2148–2166. doi:10.1002/glia.23883.
27. Landry AP, Balas M, Alli S, Spears J, Zador Z. Distinct regional ontogeny and activation of tumor associated macrophages in human glioblastoma. *Sci Rep.* 2020;10(1):19542. doi:10.1038/s41598-020-76657-3.
28. Chen Z, Ross JL, Hambarzumyan D. Intravital 2-photon imaging reveals distinct morphology and infiltrative properties of glioblastoma-associated macrophages. *Proc Natl Acad Sci USA.* 2019;116(28):14254–14259. doi:10.1073/pnas.1902366116.
29. Neftel C, Laffy J, Filbin MG, Hara T, Shore ME, Rahme GJ, Richman AR, Silverbush D, Shaw ML, Hebert CM. et al. An integrative model of cellular states, plasticity, and genetics for glioblastoma. *Cell.* 2019;178(4):835–849 e21. doi:10.1016/j.cell.2019.06.024.
30. Ravi VM, Will P, Kueckelhaus J, Sun N, Joseph K, Salié H, Vollmer L, Kuliesiute U, von Ehr J, Benotmane JK. et al. Spatially resolved multi-omics deciphers bidirectional tumor–host interdependence in glioblastoma. *Cancer Cell.* 2022;40(6):639–655 e13. doi:10.1016/j.ccell.2022.05.009.
31. Massey AJ, Cotterill S. Multiparametric cell cycle analysis using the operetta high-content imager and harmony software with PhenoLOGIC. *PLoS One.* 2015;10(7):e0134306. doi:10.1371/journal.pone.0134306.
32. Vianello C, Dal Bello F, Shin SH, Schiavon S, Bean C, Magalhães Rebelo AP, Knedlik T, Esfahani EN, Costiniti V, Lacruz RS. et al. High-throughput microscopy analysis of mitochondrial membrane potential in 2D and 3D models. *Cells.* 2023;12(7):1089. doi:10.3390/cells12071089.
33. Cancer Genome Atlas Research N. Comprehensive genomic characterization defines human glioblastoma genes and core pathways. *Nature.* 2008;455(7216):1061–1068.
34. Brennan CW, Verhaak RW, McKenna A, Campos B, Noushmehr H, Salama S, Zheng S, Chakravarty D, Sanborn J, Berman S. et al. The somatic genomic landscape of glioblastoma. *Cell.* 2013;155(2):462–477. doi:10.1016/j.cell.2013.09.034.
35. Patel AP, Tirosh I, Trombetta JJ, Shalek AK, Gillespie SM, Wakimoto H, Cahill DP, Nahed BV, Curry WT, Martuza RL. et al. Single-cell RNA-seq highlights intratumoral heterogeneity in primary glioblastoma. *Science.* 2014;344(6190):1396–1401. doi:10.1126/science.1254257.
36. Wang Q, Hu B, Hu X, Kim H, Squatrito M, Scarpace L, deCarvalho AC, Lyu S, Li P, Li Y. et al. Tumor evolution of glioma-intrinsic gene expression subtypes associates with immunological changes in the microenvironment. *Cancer Cell.* 2017;32(1):42–56 e6. doi:10.1016/j.ccell.2017.06.003.
37. Hambarzumyan D, Gutmann DH, Kettenmann H. The role of microglia and macrophages in glioma maintenance and progression. *Nat Neurosci.* 2016;19(1):20–27. doi:10.1038/nn.4185.
38. Tichy J, Spechtmeier S, Mittelbronn M, Hattingen E, Rieger J, Senft C, Foerch C. Prospective evaluation of serum glial fibrillary acidic protein (GFAP) as a diagnostic marker for glioblastoma. *J Neurooncol.* 2016;126(2):361–369. doi:10.1007/s11060-015-1978-8.
39. Kaffes I, Szulzewsky F, Chen Z, Herting CJ, Gabanic B, Velázquez Vega JE, Shelton J, Switchenko JM, Ross JL, McSwain LF. et al. Human mesenchymal glioblastomas are characterized by an increased immune cell presence compared to proneural and classical tumors. *Oncoimmunology.* 2019;8(11):e1655360. doi:10.1080/2162402X.2019.1655360.
40. Sottoriva A, Spiteri I, Piccirillo SGM, Touloumis A, Collins VP, Marioni JC, Curtis C, Watts C, Tavaré S. Intratumor heterogeneity in human glioblastoma reflects cancer evolutionary dynamics. *Proc Natl Acad Sci USA.* 2013;110(10):4009–4014. doi:10.1073/pnas.1219747110.
41. Spertini O, Cordey AS, Monai N, Giuffrè L, Schapira M. P-selectin glycoprotein ligand 1 is a ligand for L-selectin on neutrophils, monocytes, and CD34+ hematopoietic progenitor cells. *J Cell Biol.* 1996;135(2):523–531. doi:10.1083/jcb.135.2.523.
42. DeRogatis JM, Viramontes KM, Neubert EN, Tinoco R. PSGL-1 immune checkpoint inhibition for CD4(+) T cell cancer immunotherapy. *Front Immunol.* 2021;12:636238. doi:10.3389/fimmu.2021.636238.
43. Zarbock A, Müller H, Kuwano Y, Ley K. PSGL-1-dependent myeloid leukocyte activation. *J Leukoc Biol.* 2009;86(5):1119–1124. doi:10.1189/jlb.0209117.
44. Hallahan DE, Staba-Hogan MJ, Virudachalam S, Kolchinsky A. X-ray-induced P-selectin localization to the lumen of tumor blood vessels. *Cancer Res.* 1998;58(22):5216–5220.
45. Kronenberg G, Uhlemann R, Richter N, Klempin F, Wegner S, Staerck L, Wolf S, Uckert W, Kettenmann H, Endres M. et al. Distinguishing features of microglia- and monocyte-derived macrophages after stroke. *Acta Neuropathol.* 2018;135(4):551–568. doi:10.1007/s00401-017-1795-6.
46. Sorensen MD, Dahlrot RH, Boldt HB, Hansen S, Kristensen BW. Tumour-associated microglia/macrophages predict poor prognosis in high-grade gliomas and correlate with an aggressive tumour subtype. *Neuropathol Appl Neurobiol.* 2018;44(2):185–206. doi:10.1111/nan.12428.
47. Marx S, Splittstöhser M, Kinnen F, Moritz E, Joseph C, Paul S, Paland H, Seifert C, Marx M, Böhm A. et al. Platelet activation parameters and platelet-leucocyte-conjugate formation in glioblastoma multiforme patients. *Oncotarget.* 2018;9(40):25860–25876. doi:10.18632/oncotarget.25395.
48. Passacquale G, Vamadevan P, Pereira L, Hamid C, Corrigan V, Ferro A. Monocyte-platelet interaction induces a pro-inflammatory phenotype in circulating monocytes. *PLoS One.* 2011;6(10):e25595. doi:10.1371/journal.pone.0025595.
49. Komohara Y, Ohnishi K, Kuratsu J, Takeya M. Possible involvement of the M2 anti-inflammatory macrophage phenotype in growth of human gliomas. *J Pathol.* 2008;216(1):15–24. doi:10.1002/path.2370.

50. Prosniak M, Harshyne LA, Andrews DW, Kenyon LC, Bedelbaeva K, Apanasovich TV, Heber-Katz E, Curtis MT, Cotzia P, Hooper DC. et al. Glioma grade is associated with the accumulation and activity of cells bearing M2 monocyte markers. *Clin Cancer Res.* 2013;19(14):3776–3786. doi:10.1158/1078-0432.CCR-12-1940 .
51. Nguyen P, Phennicie R, Kauffman K, Nowakowska D, Zafari M, Komoroski V, Sazinsky S, Wahle J, Manfra D, Vaidya S, Brehm M. Targeting psgl-1, a novel macrophage checkpoint, repolarizes suppressive macrophages, induces an inflammatory tumor microenvironment, and suppresses tumor growth. *J Immunother Cancer.* 2020;8:A513–A513.
52. Nowakowska D, Phennicie R, Kauffman K, Zafari M, Rooney K, O’Nuallain B, Sazinsky S, Wahle J, Feldman I, Novobrantseva T. et al. PSGL-1 is a novel macrophage checkpoint in immuno-oncology. *J Clin Oncol.* 2020;38(15_suppl):e15090–e15090. doi:10.1200/JCO.2020.38.15_suppl.e15090.
53. Yuan D, Chen W, Jin S, Li W, Liu W, Liu L, Wu Y, Zhang Y, He X, Jiang J. et al. Co-expression of immune checkpoints in glioblastoma revealed by single-nucleus RNA sequencing and spatial transcriptomics. *Comput Struct Biotechnol J.* 2024;23:1534–1546. doi:10.1016/j.csbj.2024.04.014.
54. Gabrusiewicz K, Rodriguez B, Wei J, Hashimoto Y, Healy LM, Maiti SN, Thomas G, Zhou S, Wang Q, Elakkad A. et al. Glioblastoma-infiltrated innate immune cells resemble M0 macrophage phenotype. *JCI Insight.* 2016;1(2):1(2). doi:10.1172/jci.insight.85841.
55. Zheng Y, Miu Y, Yang X, Yang X, Zhu M. CCR7 mediates tgfb-1-induced human malignant glioma invasion, migration, and epithelial–mesenchymal transition by activating MMP2/9 through the nuclear factor KappaB signaling pathway. *DNA Cell Biol.* 2017;36(10):853–861. doi:10.1089/dna.2017.3818.
56. Classen A, Lloberas J, Celada A. Macrophage activation: classical versus alternative. *Methods Mol Biol.* 2009;531:29–43.
57. Zhou W, Ke SQ, Huang Z, Flavahan W, Fang X, Paul J, Wu L, Sloan AE, McLendon RE, Li X. et al. Periostin secreted by glioblastoma stem cells recruits M2 tumour-associated macrophages and promotes malignant growth. *Nat Cell Biol.* 2015;17(2):170–182. doi:10.1038/ncb3090.
58. Kralova Lesna I, Kralova A, Cejkova S, Fronck J, Petras M, Sekerkova A, Thieme F, Janousek L, Poledne R. Characterisation and comparison of adipose tissue macrophages from human subcutaneous, visceral and perivascular adipose tissue. *J Transl Med.* 2016;14(1):208. doi:10.1186/s12967-016-0962-1.
59. Chavez-Galan L, Olleros ML, Vesin D, Garcia I. Much more than M1 and M2 macrophages, there are also CD169(+) and TCR(+) macrophages. *Front Immunol.* 2015;6:263. doi:10.3389/fimmu.2015.00263.
60. Eyler CE, Wu Q, Yan K, MacSwords J, Chandler-Militello D, Misuraca K, Lathia J, Forrester M, Lee J, Stamler J. et al. Glioma stem cell proliferation and tumor growth are promoted by nitric oxide synthase-2. *Cell.* 2011;146(1):53–66. doi:10.1016/j.cell.2011.06.006.
61. Zhang Y, Boesen CC, Radaev S, Brooks AG, Fridman W-H, Sautes-Fridman C, Sun PD. Crystal structure of the extracellular domain of a human FcγRIII. *Immunity.* 2000;13(3):387–395. doi:10.1016/S1074-7613(00)00038-8.
62. Barros MH, Hauck F, Dreyer JH, Kempkes B, Niedobitek G. Macrophage polarisation: an immunohistochemical approach for identifying M1 and M2 macrophages. *PLoS One.* 2013;8(11):e80908. doi:10.1371/journal.pone.0080908.
63. Mignogna C, Signorelli F, Vismara MFM, Zeppa P, Camastra C, Barni T, Donato G, Di Vito A. A reappraisal of macrophage polarization in glioblastoma: histopathological and immunohistochemical findings and review of the literature. *Pathol Res Pract.* 2016;212(6):491–499. doi:10.1016/j.prp.2016.02.020.
64. Kelley JL, Ozment TR, Li C, Schweitzer JB, Williams DL. Scavenger receptor-A (CD204): a two-edged sword in health and disease. *Crit Rev Immunol.* 2014;34(3):241–261. doi:10.1615/CritRevImmunol.2014010267.
65. Schartner JM, Hagar AR, Van Handel M, Zhang L, Nadkarni N, Badie B. Impaired capacity for upregulation of MHC class II in tumor-associated microglia. *Glia.* 2005;51(4):279–285. doi:10.1002/glia.20201.
66. Szatmari T, Lumniczky K, Désaknai S, Trajcevski S, Hídvégi EJ, Hamada H, Sáfrány G. Detailed characterization of the mouse glioma 261 tumor model for experimental glioblastoma therapy. *Cancer Sci.* 2006;97(6):546–553. doi:10.1111/j.1349-7006.2006.00208.x.
67. Lisi L, Ciotti GMP, Braun D, Kalinin S, Currò D, Dello Russo C, Coli A, Mangiola A, Anile C, Feinstein DL. et al. Expression of iNOS, CD163 and ARG-1 taken as M1 and M2 markers of microglial polarization in human glioblastoma and the surrounding normal parenchyma. *Neurosci Lett.* 2017;645:106–112. doi:10.1016/j.neulet.2017.02.076.
68. Cannarile MA, Weisser M, Jacob W, Jegg A-M, Ries CH, Rüttinger D. Colony-stimulating factor 1 receptor (CSF1R) inhibitors in cancer therapy. *J Immunother Cancer.* 2017;5(1):53. doi:10.1186/s40425-017-0257-y.
69. Wang Q, He Z, Huang M, Liu T, Wang Y, Xu H, Duan H, Ma P, Zhang L, Zamvil SS. et al. Vascular niche IL-6 induces alternative macrophage activation in glioblastoma through HIF-2α. *Nat Commun.* 2018;9(1):559. doi:10.1038/s41467-018-03050-0.
70. Zhang QW, Liu L, Gong C-Y, Shi H-S, Zeng Y-H, Wang X-Z, Zhao Y-W, Wei Y-Q. Prognostic significance of tumor-associated macrophages in solid tumor: a meta-analysis of the literature. *PLoS One.* 2012;7(12):e50946. doi:10.1371/journal.pone.0050946.
71. Erta M, Quintana A, Hidalgo J. Interleukin-6, a major cytokine in the central nervous system. *Int J Biol Sci.* 2012;8(9):1254–1266. doi:10.7150/ijbs.4679.
72. Olmos G, Llado J. Tumor necrosis factor alpha: a link between neuroinflammation and excitotoxicity. *Mediators Inflamm.* 2014;2014:1–12. doi:10.1155/2014/861231.
73. Ziegler-Heitbrock L, Ancuta P, Crowe S, Dalod M, Grau V, Hart DN, Leenen PJM, Liu Y-J, MacPherson G, Randolph GJ. et al. Nomenclature of monocytes and dendritic cells in blood. *Blood.* 2010;116(16):e74–e80. doi:10.1182/blood-2010-02-258558.
74. De Boeck A, Ahn BY, D’Mello C, Lun X, Menon SV, Alshehri MM, Szulzewsky F, Shen Y, Khan L, Dang NH. et al. Glioma-derived IL-33 orchestrates an inflammatory brain tumor microenvironment that accelerates glioma progression. *Nat Commun.* 2020;11(1):4997. doi:10.1038/s41467-020-18569-4.
75. Takenaka MC, Gabriely G, Rothhammer V, Mascanfroni ID, Wheeler MA, Chao C-C, Gutiérrez-Vázquez C, Kenison J, Tjon EC, Barroso A. et al. Author correction: control of tumor-associated macrophages and T cells in glioblastoma via AHR and CD39. *Nat Neurosci.* 2019;22(9):1533. doi:10.1038/s41593-019-0446-8.
76. Brackmann M, Schuchmann S, Anand R, Braunewell K-H. Neuronal Ca²⁺ sensor protein VILIP-1 affects cGMP signalling of guanylyl cyclase B by regulating clathrin-dependent receptor recycling in hippocampal neurons. *J Cell Sci.* 2005;Pt 118(11):2495–2505. doi:10.1242/jcs.02376.
77. Tarawneh R, Lee J-M, Ladenson JH, Morris JC, Holtzman DM. CSF VILIP-1 predicts rates of cognitive decline in early Alzheimer disease. *Neurology.* 2012;78(10):709–719. doi:10.1212/WNL.0b013e318248e568.
78. Hausmann D, Hoffmann DC, Venkataramani V, Jung E, Horschitz S, Tetzlaff SK, Jabali A, Hai L, Kessler T, Azofín DD. et al. Autonomous rhythmic activity in glioma networks drives brain tumour growth. *Nature.* 2023;613(7942):179–186. doi:10.1038/s41586-022-05520-4.
79. Gonzalez Guerrero AM, Jaffer ZM, Page RE, Braunewell K-H, Chernoff J, Klein-Szanto AJ. Visinin-like protein-1 is a potent inhibitor of cell adhesion and migration in squamous carcinoma cells. *Oncogene.* 2005;24(14):2307–2316. doi:10.1038/sj.onc.1208476 .
80. Fu J, Fong K, Bellacosa A, Ross E, Apostolou S, Bassi DE, Jin F, Zhang J, Cairns P, de Caceres I and Braunewell KH. VILIP-1 downregulation in non-small cell lung carcinomas: mechanisms and prediction of survival. *PLoS One.* 2008;3(2):e1698.
81. Gill BJ, Pisapia DJ, Malone HR, Goldstein H, Lei L, Sonabend A, Yun J, Samanamud J, Sims JS, Banu M. et al. MRI-localized biopsies reveal subtype-specific differences in molecular and cellular composition at the margins of glioblastoma. *Proc Natl Acad Sci USA.* 2014;111(34):12550–12555. doi:10.1073/pnas.1405839111.